Research Article

Biological and dosimetric evaluation of [^{11}C]*S*-adenosyl Methionine as a potential agent for prostate cancer diagnosis

Florencia Zoppolo[1], Erick Mora-Ramirez[3,4,5], Laura Reyes[1], Elena Vasilskis[1], Andrea Paolino[1], Williams Porcal[1,2], Patricia Oliver[1], Eduardo Savio[1,*], Manuel Bardiès[3,4], Henry Engler[1].

[1] Uruguayan Centre of Molecular Imaging (CUDIM), Montevideo, Uruguay.
[2] Universidad de la República (UdelaR), Facultad de Química, Montevideo, Uruguay.
[3] Institut National de la Santé et de la Recherche Médicale (Inserm), Centre de Recherches en Cancérologie de Toulouse (CRCT), Toulouse, France.
[4] Université Toulouse III-Paul Sabatier, CRCT, Toulouse, France.
[5] Universidad de Costa Rica, CICANUM, Escuela de Física, San José, Costa Rica.

***Corresponding author**: **Corresponding author:** Eduardo Savio. Telephone: +5982 480 3238-172. Email: eduardo.savio@cudim.org
Citation: Florencia Zoppolo, et al. Biological and dosimetric evaluation of [^{11}C]S-adenosyl Methionine as a potential agent for prostate cancer diagnosis. *Cancer Research Frontiers*. 2018; 4(1): 27-44. doi: 10.17980/2018.27

Competing Interests: The authors declare no competing financial interests.
Received May 30, 2018; Revised Sept 18, 2018; Accepted Oct 1, 2018. Published Oct 19, 2018.

ABSTRACT

Introduction: [^{11}C]Choline ([^{11}C]COL) has been widely used for prostate cancer diagnosis; however, this radiopharmaceutical is not recommended for patients with a low absolute PSA value (< 1 ng/mL) due to its limited sensitivity and specificity. The enzyme glycine *N*-methyltransferase is overexpressed during prostate cancer progression. It catalyses the methylation of glycine using *S*-adenosyl methionine (SAM or AdoMet) as a substrate. The authors have previously reported the automated radiosynthesis of [^{11}C]SAM as a potential agent in the diagnosis of aggressive prostate cancer. In this study, a biological and dosimetric evaluation of [^{11}C]SAM was performed.

Results: The evaluation of [^{11}C]SAM in a control group of healthy mouse model showed a relatively high tracer uptake in the kidneys and a rapid blood clearance. Most activity was eliminated in the urine. In a PC3 prostate cancer xenograft tumour model, [^{11}C]SAM tumour uptake was significantly higher in relation to [^{11}C]COL.The human dosimetry of [^{11}C]SAM was estimated by extrapolating the preclinical results. The mean effective dose was 8.17 x 10^{-3} mSv/MBq and 2.49 x 10^{-3} mSv/MBq without and with bladder voiding, respectively. The results for kidneys in humans were comparable to those previously described for [^{11}C]COL.

Conclusions: The PET/CT studies showed a statistically higher *in vivo* tumour uptake of [^{11}C]SAM compared to [^{11}C]COL for the cancer xenograft model. The absorbed dose estimations of major organs and the effective dose were determined. The results suggested that [^{11}C]SAM may be a potential PET tracer for prostate cancer diagnosis.

Keywords: prostate cancer; Glycine N-methyltransferase; [^{11}C]SAM; PET radiotracer; small-animal PET/CT; dosimetry.

1. Introduction

Prostate cancer (PCa) is the second most frequently diagnosed solid cancer in men worldwide. It constitutes the fifth leading cause of mortality due to cancer, representing a major public health issue (1). This pathology is characterised by a heterogeneous evolution and symptomatology with

a wide range of biological behaviours (2–4), which determines important challenges related to the management of patients. PCa can be diagnosed as localised, locally advanced or metastatic (5). The treatments available for PCa in the early stages and for the locally advanced disease include active surveillance, radical treatments (prostatectomy or radiotherapy) and androgen deprivation therapy (6). In patients with the localised disease, radical therapy may be effective; however, a substantial number of patients experience biochemical recurrence. To establish the appropriate treatment strategy, it is crucial to stage PCa accurately (7,8).

Positron Emission Tomography (PET) is a molecular imaging modality that provides valuable functional and metabolic information related to organs and tissues (9,10). This imaging technique offers a useful quantitative tool for tumour biology characterisation (11). In particular, it plays a significant role in PCa detection (7,8). Several radiotracers have been investigated and developed to evaluate this pathology using PET/CT images. Some of these radiotracers are used in a clinical setting, including [^{18}F] and [^{11}C]choline ([^{11}C]COL), [^{11}C]acetate, [^{18}F]sodium fluoride and prostate-specific membrane antigen agents labelled with ^{68}Ga ([^{68}Ga]PSMA). Other radiotracers that are currently in clinical or preclinical development are prostate-specific membrane antigen agents labelled with ^{18}F ([^{18}F]PSMA), [^{18}F]fluoroethylcholine ([^{18}F]FEC), [^{18}F]FDHT (an androgen analogue, 16a-[^{18}F]-fluoro-5a-dihydrotestosterone), [^{18}F]FACBC (a L-leucine analogue, anti-1-amino-3-[^{18}F]-fluorocyclobutane-1-carboxylic acid) and bombesin analogues (3,7,12–14).

[^{11}C]COL is one of the most widely used radiopharmaceutical for PCa diagnosis. Due to its limited sensitivity and specificity, its role in the primary staging of PCa is still under debate (8,12). The clinical application of [^{11}C]COL aims to restage patients who suffer from biochemical recurrence; however, the detection sensitivity of [^{11}C]COL decreases with low prostate-specific antigen (PSA) values. Hence, this tracer is not applicable for patients who present an absolute PSA value of < 1 ng/mL (15).

A previous study described the overexpression of glycine N-methyltransferase (GNMT EC 2.1.1.20) in most PCa cells, especially in PC3 line, compared with normal prostate epithelial cells. According to these findings, the silencing of GNMT expression by siRNA induces apoptosis in more aggressive PCa cell (as PC3) compare to less aggressive androgen-dependent LNCaP (16). In addition, based on an investigation carried out from PCa tissue, they concluded that higher GNMT cytoplasmic expression was associated with a higher Gleason score and higher pT stage. This enzyme is involved in the methylation catalysis of glycine to produce sarcosine using *S*-adenosyl methionine (SAM or AdoMet) as a substrate. As a result, the increased levels of GNMT cause an accumulation of sarcosine. It is important to note that this metabolite plays an intermediary role in cancer invasion and aggressiveness (17).

The development of new PET tracers to improve sensitivity and specificity for PCa detection in patients with biochemical failure, who progresses with an aggressive pattern, is crucial.

The authors recently reported the automated one-pot radiosynthesis of [^{11}C]SAM as a potential agent that can be used to evaluate the expression level of GNMT in tumour tissues, especially in the diagnosis of aggressive PCa (18).

In a previous study, Ishiwata and colleagues described the biodistribution of [^{11}C]SAM in healthy rats and one rabbit (19). Another group investigated the tumour accumulation of [^{11}C]SAM in two animal models: mice bearing mammary carcinoma and rats bearing ascitic hepatoma. They concluded that the tracer could be useful for locating tumours whose transmethylation activity is modified (20).

The aim of this article is to discuss the evaluation of the biological behaviour of [^{11}C]SAM as well as its tumour uptake through *ex vivo* biodistribution and *in vivo* PET/CT imaging studies. The biological evaluation was performed using two mice models: a healthy model and a PC3 human prostate cancer xenograft model. To examine the role of [^{11}C]SAM as a prostate cancer imaging agent, the tracer was compared to [^{11}C]COL, which was selected as a reference. In addition, the human radiation dosimetry of [^{11}C]SAM was estimated by extrapolating preclinical results to humans.

2. Materials and methods

2.1 *Materials*

All chemicals, solvents and reagents were purchased from commercial sources (ABX, Sigma-Aldrich,

Merck, Carlo Erba and Dorwil). They were analytical grade and were used without further purification. The Sep-Pak Classic Accell Plus CM cation-exchange cartridges and the 0.22 µm sterilising filters were purchased from Waters, whereas the Strata XC-SPE cartridges and the semipreparative HPLC column (a 250/10 mm Luna 5 µm C_{18}) were purchased from Phenomenex. The analytical HPLC column was an EC 250/4.6 mm Nucleodur 100-5 C_{18}ec from Macherey-Nagel.

2.2 *Radiochemical synthesis*

The synthetic processes were performed using a TRACERlab® FX C Pro automated platform (GE Healthcare). [^{11}C]CO_2 was produced in a PET Trace® 16.5 MeV cyclotron (GE Healthcare).

[^{11}C]COL was synthesised according to the method reported by Shao *et al.* (21). [^{11}C]CH_3I was used as a methylating agent for the labelling reaction. [^{11}C]CH_3I, produced in the module, was passed through a CM Sep-Pak cartridge loaded with the precursor *N*,*N*-dimethyl ethanolamine (40 µL). The cartridge was washed with ethanol (10 mL) followed by water for injection (10 mL). The trapped product was eluted and formulated with 0.9% NaCl (10 mL). The final solution was transferred to a sterile vial through a 0.22 µm sterilising filter and submitted for quality control testing. The obtained compound was analysed by HPLC (Shimadzu UFLC equipped with diode array, conductivity and gamma detectors) using the following conditions: NaH_2PO_4 0.05 M as the mobile phase and an isocratic flow rate of 0.8 mL/min on a C_{18} analytical column. Chromatograms were registered using UV (200 nm), conductivity and gamma detectors. The tracer was obtained with a radiochemical purity of > 90%.

[^{11}C]SAM was obtained via the *S*-methylation reaction of *S*-adenosyl homocysteine (SAH) with [^{11}C]CH_3OTf (^{11}C-methylating agent). This synthesis was performed according to the procedure described previously (18). The [^{11}C]CH_3OTf produced in the module was bubbled into a reactor loaded with the precursor solution (5 mg of SAH dissolved in 400 µL of formic acid). Then, the reaction mixture was heated at 60 ºC for 1 min. After that, the desired ^{11}C-labelled compound from the reactor was purified using a semi-preparative HPLC (conditions: C_{18} semi-preparative column, 0.1 M sodium acetate buffer pH 4.5: acetonitrile (98:2) as the mobile phase, isocratic flow rate of 6.0 mL/min, UV (254 nm) and gamma detectors). The fraction containing [^{11}C]SAM was collected and purified using a Strata XC-SPE cartridge. The product was eluted with Na_2HPO_4 0.1 M pH 8.5: EtOH (9:1) (4 mL) and formulated in 0.9% NaCl (6 mL). The solution was then transferred to a sterile vial through a 0.22 µm sterilising filter. The final product was analysed by HPLC employing the following conditions: 50 mM ammonium acetate buffer pH 5.4 with 1% TFA as the mobile phase A and acetonitrile as the mobile phase B. The elution gradient was isocratic at 0% B from 0 to 15 min, and then it was increased linearly from 0 to 100% B from 15 to 20 min. The flow rate employed was 2 mL/min on a C_{18} analytical column. Chromatograms were registered using UV (260 nm) and gamma detectors. The global radiochemical purity of the resultant compound was > 90%, and the specific activity ranged from 207 to 1363 GBq/µmol (this value was determined taking only the [^{11}C](*S, S*)-SAM isomer into account).

2.3 *Animals and tumour cell line*

Male Swiss and Nude N: NIH (S) – Foxn 1^{nu} mice 13-18 weeks old were used as the healthy control and prostate cancer tumour models, respectively, for the *ex vivo* and *in vivo* studies. Animals were housed in pairs in racks with filtered air under controlled conditions (temperature [24 ± 1] ºC and relative humidity [40-60]%). They were maintained at 14:10 h light/dark cycles in the CUDIM animal facility with food and water *ad libitum*.

The animal experimentation protocol was designed in accordance with institutional, national and international guidelines for the use of research animals. It was approved by the Ethical Committee of CUDIM (No. 14012202) in agreement with national regulations: national law on animal experimentation No. 18.611, Commission of Ethics for Animal Studies (CEUA) and National Commission of Experimentation with Animals (CNEA).

For the development of a xenograft human prostate cancer model, a PC3 human prostate cancer cell line (ATCC ATCC® CRL-1435™) was purchased from American Type Culture Collection Cell. The cells were cultured in Dubelcco's modified Eagle's medium high glucose (DMEM, Capricorn Scientific) supplemented with 10% (v/v) foetal bovine serum (FBS, Gibco) and an antibiotic/antimycotic solution. The cells were grown to confluence in cell culture T-flasks in a humidified atmosphere of 5% CO_2 at 37 ºC.

2.4 *Cell transplantation*

A xenograft human prostate cancer mice model was used as the prostate cancer tumour model. Three million PC3 cells suspended in 0.9% NaCl (100-200 µL) were injected subcutaneously into the right upper leg of male Nude mice (9–12 weeks old). Appropriate tumour volumes (100–350 mm^3) were achieved between four to six weeks post-inoculation. The tumours were measured once per week with a micro calliper in two dimensions, and the tumour volumes were calculated as (smaller diameter)^2 x larger diameter x $\pi/6$.

2.5 *Ex vivo biodistribution studies*

Biodistribution studies were performed for both the control and the PC3 tumour-bearing mice. A solution of [^{11}C]SAM (7.7-36.0 MBq, 100-200 µL) was injected intravenously (iv) in the control group (15-16 weeks old, 32.9-38.8 g) and in the tumour-bearing mice (13-18 weeks old, 21.5-27.1 g) via the tail vein. Mice were sacrificed by cervical dislocation at 10, 30 and 70 min after injection for the control group and 14, 30 and 70 min for the tumour-bearing group. Different organ and tissue samples were removed (blood, liver, heart, lungs, spleen, kidneys, muscles, bones, stomach, gastrointestinal tract, carcass, bladder and urine). In the case of xenograft tumour mice, the excised tumour was also removed. The removed samples, including the tumours, were weighed, and the radioactivity was measured by a gamma counter (3" x 3" well type NaI(Tl) solid scintillation detector coupled to a multichannel analyser ORTEC). The percentage of injected activity per gram of tissue (% IA/g) and the percentage of injected activity in the whole organ (% IA) were calculated as well as the target to non-target (T/NT) ratio from the tumour to the muscle. Corrections for the different sample geometries were applied when necessary.

2.6 In vivo *PET/CT Imaging studies*

PET/CT scans were performed using a small animal tri-modality PET/SPECT/CT scanner (Triumph^{TM}, TriFoil, Inc., US) based on Quad-APD detector modules coupled with LYSO/LGSO scintillators (spatial resolution: 1.0 mm; axial field of view (FOV): 3.75 cm).

Data were acquired in a list mode in a 184 x 184 x 31 matrix with a pixel size of 0.25 x 0.25 x 1.175 mm and a coincidence window width of 22.22 nsec. The animals were anesthetised with 2% isoflurane in an oxygen flow of 2 L/min, placed in a prone position on the scanner bed and injected iv into the tail vein with 100-200 µL of [^{11}C]SAM (18.3-50.4 MBq) or [^{11}C]COL (15.3-35.7 MBq). [^{11}C]COL was only examined for the PC3 tumour-bearing mice model to be compared with [^{11}C]SAM.

For the xenograft tumour mice, images were obtained when tumours reached an optimum size (100–350 mm^3, 13–18 weeks old). The control group was scanned at the same age. PET dynamic image acquisition began at t=0 min after radiotracer administration and was performed during 60 min for the tumour model (1 frame × 5 min, 1 frame × 15 min, 2 frames × 20 min). For the control group, PET static image acquisition began at t=5 min after radiotracer administration and was performed for 5 min followed by two additional statics acquisitions of 20 min each. The CT examination was performed for 1.98 min (field of view = 4.7 cm). The mice were scanned in a random order.

Sinograms were reconstructed using 3D maximum likelihood expectation maximisation (3D-MLEM) with 30 iterations.

Image processing and a semi-quantitative analysis were carried out using PMOD software, v.3.4. (PMOD Technologies, Ltd., Zurich, Switzerland). PET studies were co-registered with the corresponding CT scan study for anatomical localisation. Images were displayed as coronal, sagittal and axial slices. Volumes of interest (VOIs) were drawn manually over the different organs (brain, heart, lung, liver, kidney, bladder, bone and muscle for the control group; tumour and contralateral muscle for tumour-bearing mice) to generate time-activity curves and to calculate T/NT ratios. The activity concentration within each VOI was expressed as the hot spot average (five pixels of the hot spot) in the case of the tumour model and as the average over the whole VOI for the control group (kBq/cc). The percentage of activity in each organ was calculated considering the sum of the activity of all analysed samples.

2.7 *Statistical analysis*

The results were expressed as mean ± standard deviation (SD) for the biodistribution and image studies. The unpaired Student's *t*-test was used to compare the radiotracer uptake in the tumour regions. *p* values <0.05 were defined as statistically significant.

(a)

Tissue	[^{11}C]SAM uptake [A]		
	10 min[B]	30 min[B]	70 min[C]
Blood	4.43 ± 0.55	2.00 ± 0.77	0.84 ± 0.37
Liver	1.46 ± 0.24	0.92 ± 0.19	0.71 ± 0.10
Heart	1.15 ± 0.10	0.50 ± 0.05	0.25 ± 0.06
Lung	2.56 ± 0.33	1.09 ± 0.09	0.43 ± 0.06
Spleen	0.93 ± 0.10	0.62 ± 0.22	0.46 ± 0.02
Kidney	16.17 ± 1.64	19.43 ± 1.20	8.63 ± 0.21
Muscle	0.65 ± 0.12	0.26 ± 0.06	0.23 ± 0.16
Bone	0.87 ± 0.10	0.36 ± 0.04	0.36 ± 0.28

[A] Results are expressed as mean % IA/g ± SD; [B] n=3; [C] n=2.

(b)

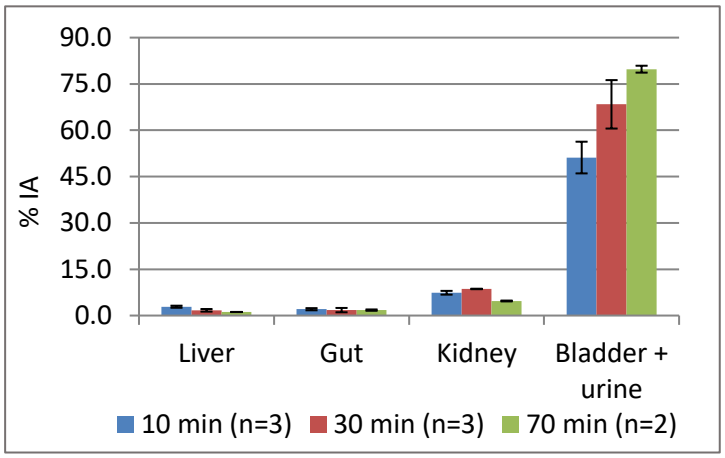

Figure 1. (a) Biodistribution data of [^{11}C]SAM in the control group. (b) Elimination profile of [^{11}C]SAM in the control group based on biodistribution studies. All measurements were performed using a gamma counter.

2.8 *Percentage of injected activity, residence time and absorbed dose calculations*

According to the MIRD Radionuclide Data and Decay Schemes (22), the physical half-life of ^{11}C is 20.39 min. Eight mice were used for dosimetry purposes, three for t=10 min, three for t=30 min and two for t=70 min. Three times were registered: injection time (t_{inj}), sacrifice time (t_{sac}) and organ/tissue measuring time (t_{mes}). All organs/tissues were weighed. The organs included in this study were blood, liver and gallbladder, heart, lungs, spleen, kidneys, muscles, bones, stomach, intestines, carcass and bladder+urine.

2.8.1 Percentage of injected activity calculation

All organ measurements were estimated in units of counts per second in an activimeter ORTEC Lab. The percentage of injected activity $\left(\%A_{inj}\right)_{t_i}^{organ}$ for each organ/tissue at one particular time (t_i=10, 30, 70 min) can therefore be expressed as shown in equation 1:

$$\left(\%A_{inj}\right)_{t_i}^{organ} = \frac{\left(cps_{bk,geo}\right)^{t=t_{mes}} * e^{\lambda(t_{mes}-t_{sac})}}{\sum_{organ}\left(cps_{bk,geo}\right)^{t=t_{mes}} * e^{\lambda(t_{mes}-t_{inj})}} * 100$$

The average of percentage of injected activity for each organ mouse $\overline{\left(\%A_{inj}\right)_{t_i}^{organ}}$ was also estimated for each mouse time group. The determination of equation 1 can be seen in more detail in the publication from *Kreimerman et al.* (23).

(a)

Tissue	[11C]SAM uptake [A]		
	14 min[B]	30 min[B]	70 min[C]
Blood	4.43 ± 0.98	1.94 ± 0.78	1.43 ± 0.94
Liver	1.29 ± 0.35	0.98 ± 0.08	0.78 ± 0.17
Heart	1.34 ± 0.47	0.50 ± 0.12	0.37 ± 0.16
Lung	2.13 ± 0.50	1.07 ± 0.24	0.64 ± 0.31
Spleen	0.92 ± 0.29	0.47 ± 0.04	0.48 ± 0.16
Kidney	15.49 ± 2.93	13.40 ± 3.36	12.03 ± 2.21
Muscle	0.67 ± 0.25	0.27 ± 0.06	0.18 ± 0.08
Bone	0.92 ± 0.39	0.40 ± 0.09	0.30 ± 0.14
Tumour	2.43 ± 0.40	0.90 ± 0.11	0.58 ± 0.32
T/NT ratio	3.93 ± 1.27	3.37 ± 0.36	3.14 ± 0.69

[A] Results are expressed as mean % IA/g ± SD; [B] n=3; [C] n=5.

(b)

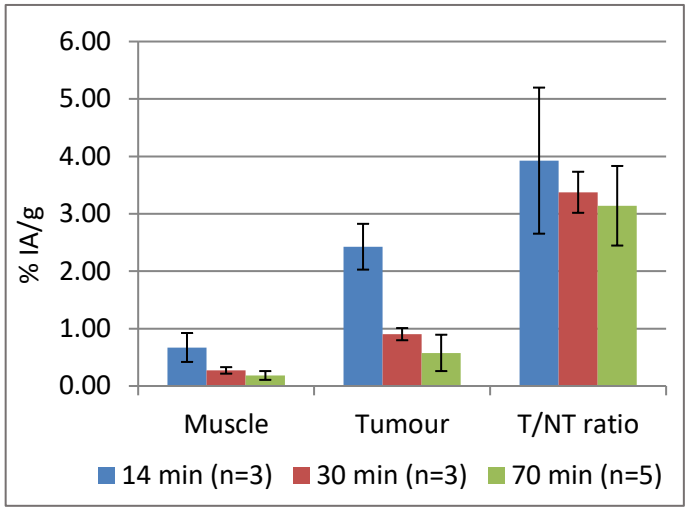

Figure 2. (a) Biodistribution data of [^{11}C]SAM in PC3 tumour-bearing mice. (b) Evolution of % IA/g over time for muscle, tumour and T/NT ratios in PC3 tumour-bearing mice after iv injection of [^{11}C]SAM based on biodistribution studies. All measurements were performed using a gamma counter.

2.8.2 Residence time calculation

An assumption of no activity at t=0 min was considered. Normalised non-decay corrected time activity curves were generated for each organ. Residence times were estimated for each organ and for each mouse time group using the trapezoidal method as described in a previous publication (24). All mathematical processing was carried out using Wolfram Mathematica (25). It was assumed that no bladder voiding may lead to an overestimation of the irradiation delivered by the bladder content. Therefore, an alternative estimation of the bladder content residence time was performed by considering bladder voiding at different times.

Normalised cumulated activity for humans was calculated using mass scaling between mice and humans for the whole body and different organs. McParland (26) described the estimation of the normalised cumulated activity for humans. Based on this information, the normalised cumulated activity for humans can be re-written as shown in equation 2:

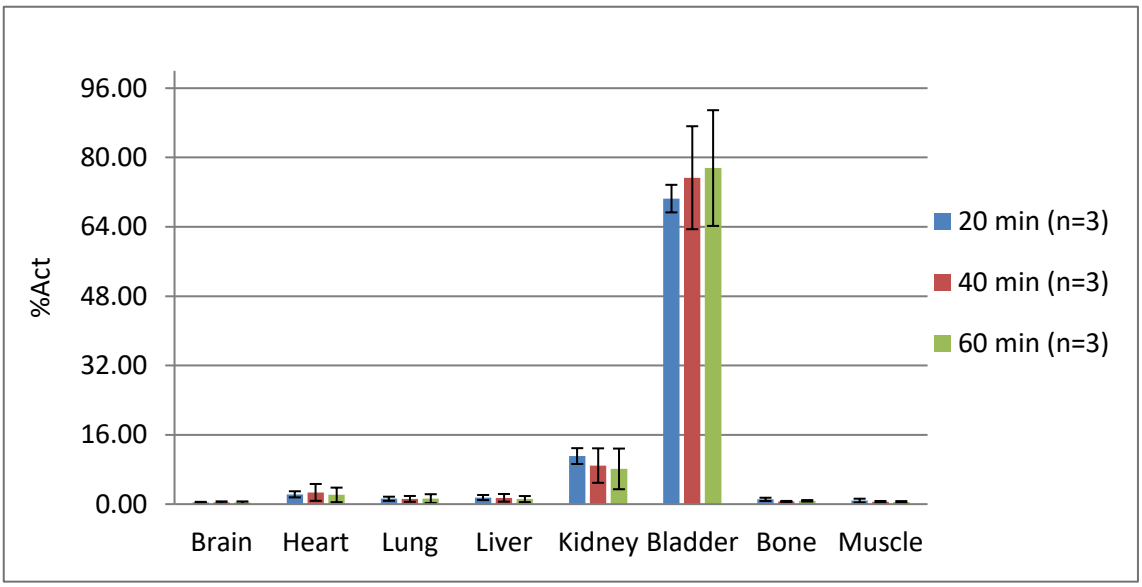

Figure 3. Time-activity curve for different organs in the control group after iv injection of [^{11}C]SAM based on imaging studies.

$$\tilde{A}_{Organ,Human} = \left(\frac{m_{Animal}}{m_{Human}}\right)_{WB} * \left(\frac{m_{Human}}{m_{Animal}}\right)_{Org} * \tilde{A}_{Organ,Animal}$$

To perform dosimetric extrapolations for humans, two versions of OLINDA were available. OLINDA/EXM V1.0 (27) and OLINDA/EXM V2.0 (28,29) provide information regarding human organ mass. OLINDA/EXM V1.0 considers the Cristy and Eckerman mathematical dosimetric models and information from ICRP-23 (30), and OLINDA/EXM V2.0 considers ICRP-89 information (31) and from this data NURBS dosimetric models were created (32). OLINDA/EXM V2.0 provides information regarding human bladder content mass and also for a 35 g total mouse body mass. This means that bladder and bladder content can be dealt with as explicit sources using OLINDA/EXM V2.0, whereas they should be integrated into the 'remainder' for OLINDA/EXM V1.0. OLINDA/EXM V2.0 was used to appraise absorbed doses that would be delivered to a human with a remainder residence time that accounts for blood, muscles, bones, stomach, carcass and intestines. Considering that the urine remaining in the bladder may lead to overestimate the irradiation, residence times were extrapolated from mice with and without considering bladder voiding.

2.8.3 Absorbed dose estimations

Using the mass scaling results and to calculate the absorbed doses for a selected group of organs, the two versions of OLINDA/EXM were used. In terms of effective dose, OLINDA/EXM V1.0 and OLINDA/EXM V2.0 follow recommendations from ICRP-60 (33) and ICRP-103 (34), respectively. All results from OLINDA/EXM V1.0 are available in the supplementary data. Hereafter, OLINDA/EXM V2.0 is referred as OLINDA.

3. Results and discussion

3.1 Ex vivo *studies*

The biological behaviours of [^{11}C]SAM were evaluated based on biodistribution studies in healthy mice (control group) and in PC3 tumour-bearing mice (prostate cancer model).

The biodistribution of [^{11}C]SAM in the control group was carried out at 10, 30 and 70 min after its administration. These results are summarised in Figure 1. The tracer concentration in kidneys was relatively high, reaching a maximum of (8.61 ±

(a)

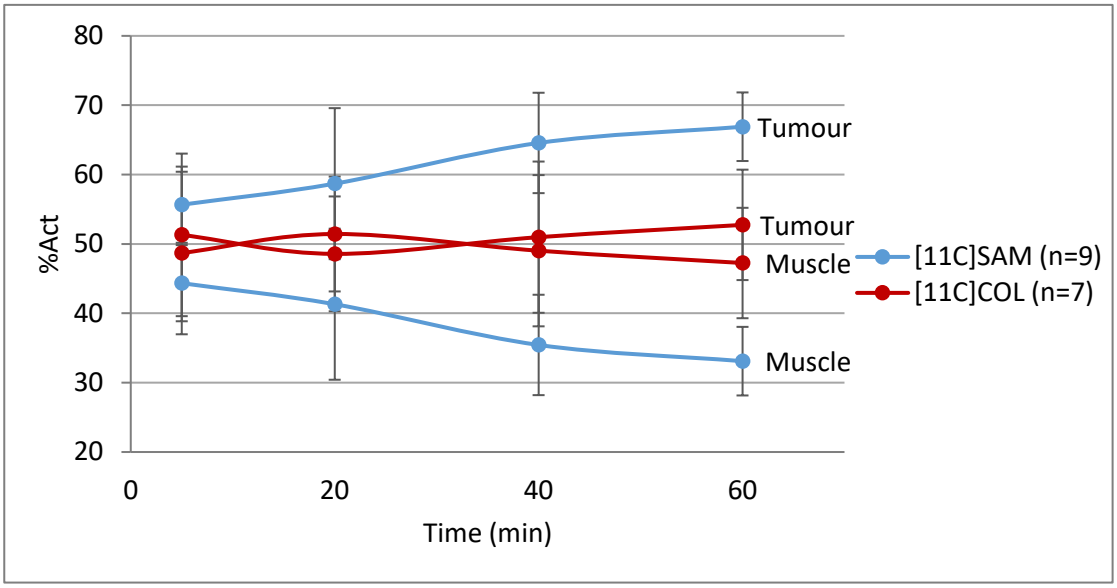

(b)

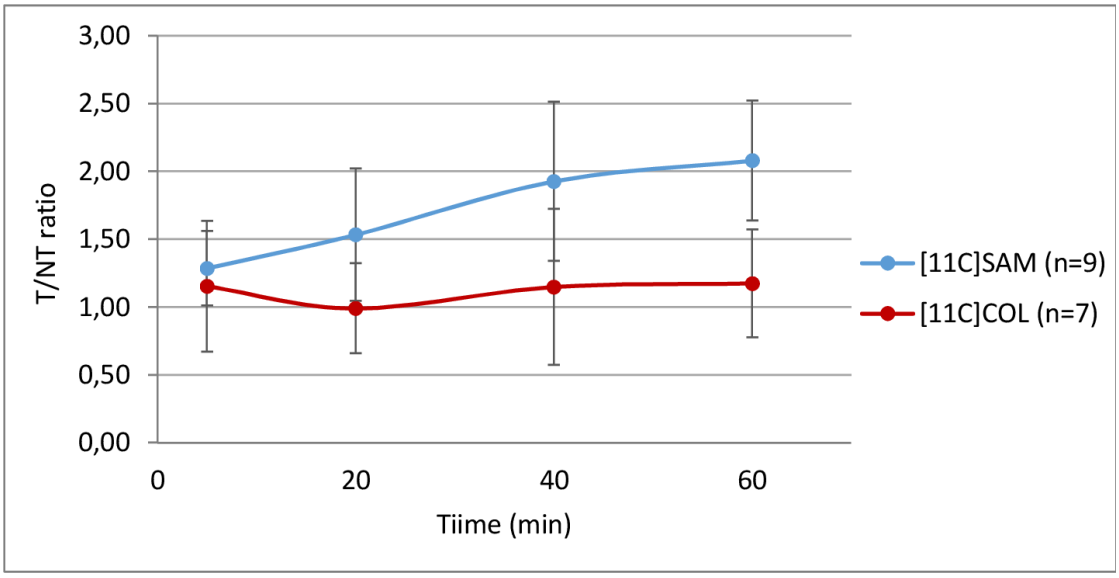

Figure 4. (a) Time-activity curves for tumour and muscle uptake for [^{11}C]SAM and [^{11}C]COL in PC3 tumour-bearing mice based on imaging studies. [^{11}C]SAM tumour uptake values were significantly higher than the contralateral muscles values ($p<0.05$). [^{11}C]COL tumour and muscle uptake values did not show significantly difference ($p>0.05$). (b) Time course of T/NT ratios (tumour to muscle) for [^{11}C]SAM and [^{11}C]COL in PC3 tumour-bearing mice based on imaging studies. [^{11}C]SAM uptake was significantly higher compared to the reference compound ($p<0.05$), except for 5 min ($p>0.05$).

0.08)% of IA at 30 min post-injection with subsequent decreasing to (4.72 ± 0.14)% IA at 70 min. The highest accumulation of [^{11}C]SAM was observed in the bladder and urine. In contrast, the uptake in the liver and gut remained low and constant throughout the study (Figure 1b). These results suggested that the elimination of the tracer was mainly caused by urinary excretion, which is in concordance with the high hydrophilicity of this compound (log P_{OCT} = -2.01 ± 0.07 (18)). This

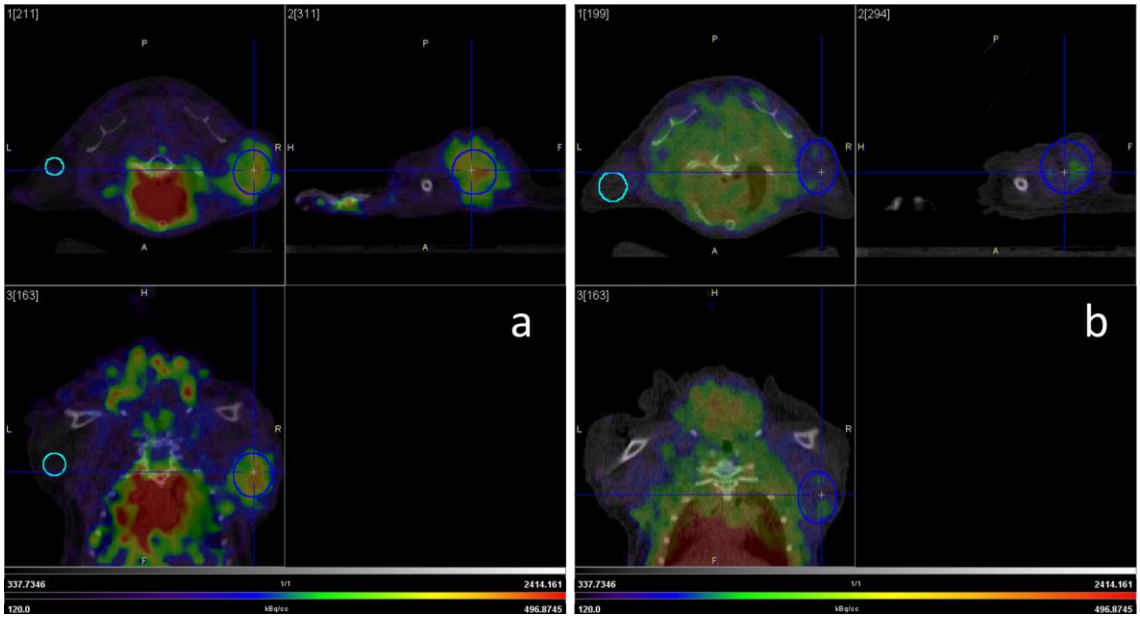

Figure 5. Coronal (top left), sagittal (top right) and axial (bottom) micro PET/CT image examples comparing [^{11}C]SAM (a) and [^{11}C]COL (b) tumour uptake in PC3 tumour-bearing mouse at 60 min of acquisition. The tumour area is displayed in blue circles; the contralateral muscle area is displayed in light blue circles. [^{11}C]SAM tumour uptake was significantly higher (p<0.05) compared to [^{11}C]COL.

elimination profile was consistent with a previous study in which the distribution of [^{11}C]SAM was reported in rats. It was also found that part of the tracer activity in the kidneys reflected renal excretion, whereas the other fraction indicated transmethylation reactions (19).

The % IA in the bladder and urine was high at 10 min after injection (> 50% IA), increasing over time to up to 80% at 70 min (Figure 1b).

The concentration of [^{11}C]SAM in blood decreased with time from (4.43 ± 0.55)% IA/g at 10 min after injection and remaining (0.84 ± 0.37)% IA/g at 70 min (Figure 1a). A rapid blood clearance of the tracer was verified. The compound did not show a high uptake in organs such as the heart, lungs, spleen, muscles or bone (Figure 1a).

To assess the tracer tumour uptake, biodistribution studies of [^{11}C]SAM were performed for the prostate cancer model. The assays were conducted at 14, 30 and 70 min after tracer administration (Figure 2).

In this model, the biodistribution pattern was similar to that observed in the control group. Significant tracer accumulation was found in the kidneys. The highest uptake was detected in the bladder and urine from (53.22 ± 14.91)% IA at 14 min post-injection to (78.47 ± 6.41)% IA at 70 min. A rapid blood clearance of the tracer was verified, and there was no high uptake in the other organs (Figure 2a). To obtain good quality PET images is important that the tracer remains in the body only for the time necessary to perform the study without showing secondary uptakes. This also means that irradiation would be low, as it is in the case of equivalent diagnostic tracers. A low background uptake generates a T/NT ratio adequate for a better PET image quality.

The tracer uptake in the tumour was compared to the muscles (reference tissue). The accumulation in the tumour was significantly higher compared to the muscles at all analysed times (p<0.05) (Figure 2b). At 14 min post-injection, the mean value of the T/NT ratios was 3.93 ± 1.27, decreasing to 3.37 ± 0.36 at 30 min and remaining thereafter relatively constant (3.14 ± 0.69) up to 70 min (see Figure 2a).

3.2 In vivo *PET/CT imaging*

Micro-PET/CT images were obtained to evaluate the distribution of [^{11}C]SAM in the control group as well

(a)

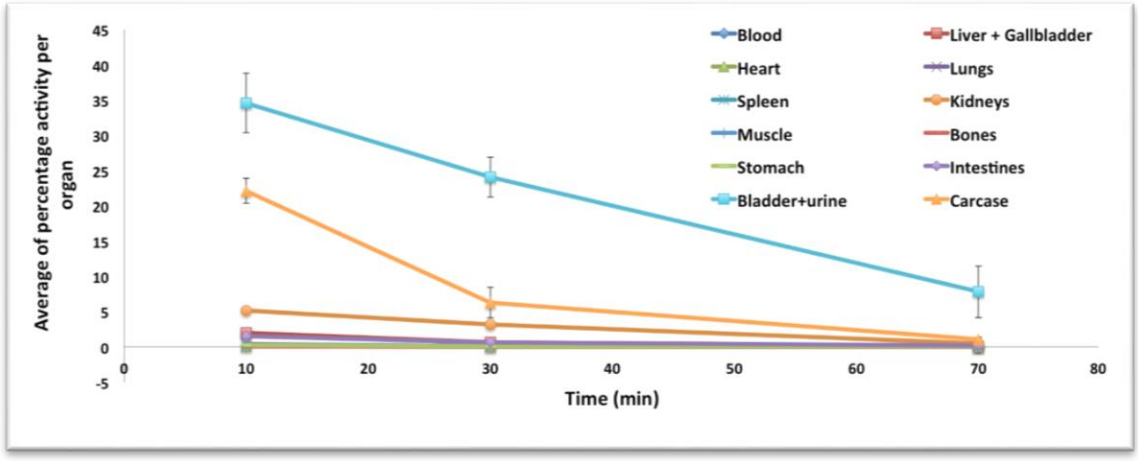

(b)

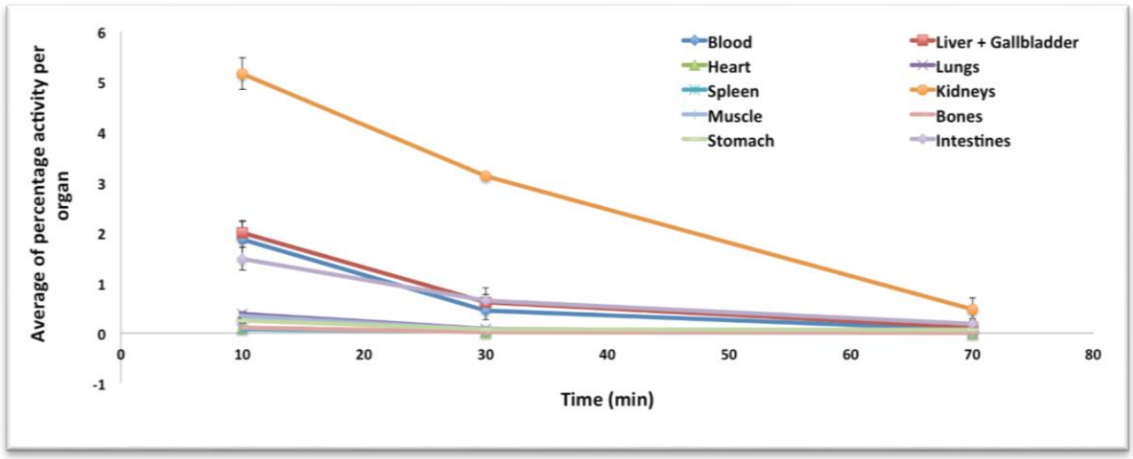

(c)

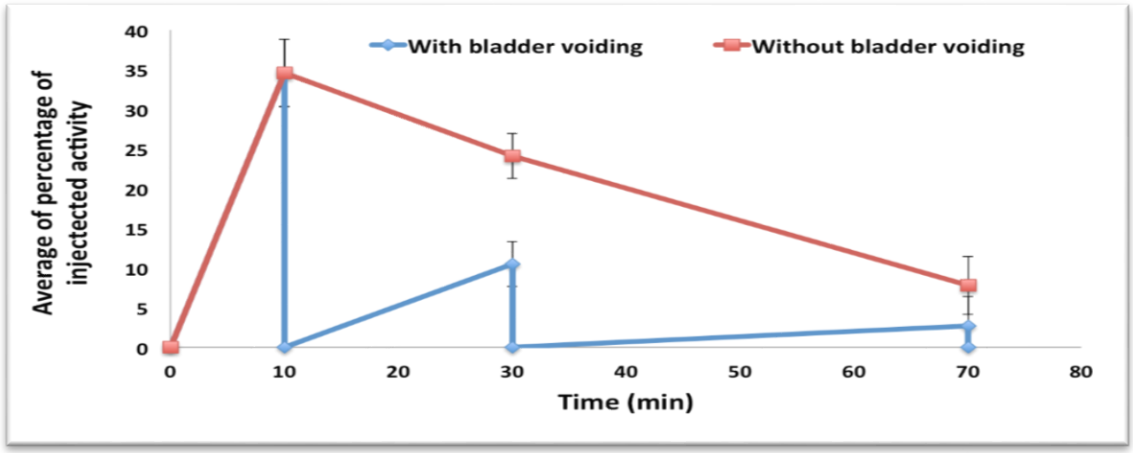

Figure 6. Average percentage of injected activity per organ for [^{11}C]SAM per mice time group based on biodistribution studies. (a) All measured organs; (b) all organs except bladder+urine and carcase; (c) bladder+urine compartment with and without bladder voiding. All measurements were performed using a gamma counter.

as in PC3 tumour-bearing mice. Static and dynamic PET scans were performed followed by a CT examination. In agreement with the biodistribution results, the control group image studies displayed a high urinary accumulation of the tracer (kidney and bladder) (Figure 3).

Table 1. Residence times (T) for each mice organ ([^{11}C]SAM).

Organ	Residence Time (h)
Blood	7.14E-03
Liver-Gallbladder	8.53E-03
Heart	4.22E-04
Lungs	1.40E-03
Spleen	3.43E-04
Kidneys	3.03E-02
Muscle	1.27E-03
Bones	4.20E-04
Stomach	1.24E-03
Intestines	7.65E-03
Carcass	9.06E-02
Bladder+urine (without bladder voiding)	2.36E-01
Bladder+urine (with bladder voiding)	5.54E-02
Remainder[A]	3.45E-01

[A] Remainder is the sum of blood, muscles, bones, stomach, carcass, intestine and bladder+urine (without bladder voiding) residence times.

[^{11}C]COL was selected as the reference radiotracer to assess the role of [^{11}C]SAM as a potential prostate cancer imaging agent in PC3 tumour-bearing mice. The tumour, muscle and T/NT dynamic profiles were compared using time-activity curves (Figure 4). In the case of [^{11}C]SAM, the PET studies showed a significantly higher tumour uptake compared to the contralateral muscles (p<0.05) (Figure 4a). The concentration of the tracer in the tumour increased over time, whereas the muscle uptake decreased, providing a mean T/NT ratio of 2.08 ± 0.44 at 60 min. In relation to [^{11}C]COL (Figure 4a), tumour and muscle uptake followed a similar pattern, which is reflected by the lower mean T/NT ratio (1.17 ± 0.40 at 60 min of acquisition).

The T/NT ratio obtained for [^{11}C]SAM increased throughout the study (Figure 4b). This was consistent with the uptake profile previously described. The time course of the T/NT ratio of [^{11}C]SAM was higher compared to [^{11}C]COL, which presented a relatively constant pattern over time. Except at the 5 min time point, [^{11}C]SAM uptake was significantly higher (p<0.05) compared to the reference compound (Figure 5). This can be explained by the initial blood distribution. These results indicate a statistically higher *in vivo* tumour uptake of [^{11}C]SAM compared to [^{11}C]COL in the PC3 prostate cancer xenograft model.

Currently those patients who suffer progressive metastatic castration-resistant prostate cancer, which is a highly lethal disorder, could benefit from new therapeutic agents with radiometabolic therapy.Lutetium-177 [^{177}Lu]PSMA-617, a radiolabelled small molecule, binds with high affinity to prostate-specific membrane antigen (PSMA) enabling beta particle therapy targeted to metastatic castration-resistant prostate cancer. There are several ongoing clinical trials to assess the benefit in terms of safety, efficacy, and effect on quality of life of this alternative in men with metastatic castration-resistant prostate cancer who progressed after standard treatments (35). [^{11}C]SAM would play an important role identifying those patients who would evolve with an aggressive prognosis and so could be candidates for a radiometabolic therapy in earlier stages of the disease.

3.3 *Residence times and absorbed dose estimations*

Regarding the data acquisition and/or measuring times for short-lived radionuclides, McParland (26) provided two recommendations: a) include data measurements between 2 and 5 min to determine the uptake of the radiopharmaceutical and b) the last point measurement should be at t=4*$T_{1/2p}$ (four

Table 2. Mass values used for mass scaling to determine male residence times.

Organ	OLINDA/EXM			
	M_{male} (g)	S-factor[A] (mGy/MBq-s)	M_{mouse} (g)	T_{male}(h)
Heart Wall	330	2.11E-4	0.1400	5.03E-04
Kidneys	310	2.36E-4	0.4746	1.00E-02
Liver+ Gallbladder[B]	1858	4.91E-5	1.8355	4.36E-03
Lungs	1200	5.72E-5	0.2018	4.20E-03
Spleen	150	4.77E-4	0.1109	2.34E-04
Bladder Contents without Bladder Voiding	211	1.91E-4[C]	0.1000	2.52E-01
Bladder Contents with Bladder Voiding	211	1.91E-4	0.1000	5.90E-02
Remainder	68941	---	34.0023	1.11E-01[D]
Whole Body	73000	1.65E-6	36.8650	-----

[A] S-factor refers to self-irradiation; [B] S-factor (self-irradiation) for liver only; [C] S-factor for urinary bladder wall considering urinary bladder content as a source; [D] Remainder takes into account blood, muscles, bones, stomach, carcass and intestines.

times the physical half-life); however, Ishiwata *et al*. reported an increase in ^{11}C concentration until 10 min after injection in rats (19). Therefore, the acquisition/measuring began at t=10 min in the current study.

The variations of the average percentages of injected activity for all organs for each mice time group are shown in Figure 6a. The excretion of radioactive material was observed in the bladder+urine compartment. The difference between the organs with the highest average percentage of injected activity was approximately 12.44% at t=10 min (bladder+urine and carcass).

The average percentage of injected activity without the contribution of the bladder+urine is provided in Figure 6b. The organs with the highest activity uptake at t=10 min were the carcass and kidneys. The variations of the average percentages of injected activity in the bladder+urine compartment with and without bladder voiding are provided in Figure 6c.

The kidneys had a high activity uptake at t=10 min, which is in agreement with previous studies on rats (Ishiwata *et al.* and Tolvanen *et al*.) (19,36).

In another article, Ishiwata *et al*. (20) described a high uptake in the kidneys and a rapid blood clearance for the same tracer in mice and rats bearing tumour cells. Looking at figure 6b, other organs with high activity uptakes were the liver-gallbladder, blood and intestines. For the same figure, rapid clearance of the tracer in blood can be seen.

For ^{11}C-radiopharmaceuticals, Tolvanen *et al*. (36) discussed different scaling methods and discrepancies between species (rats vs humans). In particular, there are qualitative differences in liver metabolism between species. Other scaling methods can be also tested. Regarding the discrepancies between species, they mentioned that due to the faster physiology of rodents, the absorbed dose and effective doses extrapolated from mice may be lower than in data obtained directly from humans. A recent publication from Avila-Rodriguez *et al*. (37) that examined other isotopes, describes that differences in sizes between species can also create discrepancies. Therefore, it is important that studies in humans validate the

Table 3. Absorbed and effective dose estimations for adult male phantom from OLINDA/EXM V2.0.

Target Organ	Male – OLINDA/EXM V 2.0			
	Without Bladder Voiding		With Bladder Voiding	
	Total (mGy/MBq)	Effective Dose ICRP-103 (mSv/MBq)	Total (mGy/MBq)	Effective Dose ICRP-103 (mSv/MBq)
Adrenals	1.81E-03	1.68E-05	1.62E-03	1.49E-05
Brain	6.23E-04	6.23E-06	6.22E-04	6.22E-06
Esophagus	8.32E-04	3.33E-05	7.87E-04	3.15E-05
Eyes	6.33E-04	---	6.25E-04	---
Gallbladder Wall	1.45E-03	1.33E-05	1.27E-03	1.17E-05
Left Colon	1.51E-03	7.31E-05	1.04E-03	5.03E-05
Small Intestine	2.44E-03	2.25E-05	1.23E-03	1.14E-05
Stomach Wall	9.34E-04	1.12E-04	8.61E-04	1.03E-04
Right Colon	1.55E-03	7.54E-05	1.03E-03	4.98E-05
Rectum	6.58E-03	1.51E-04	2.15E-03	4.94E-05
Heart Wall	8.66E-04	7.99E-06	8.25E-04	7.61E-06
Kidneys	9.19E-03	8.48E-05	8.93E-03	8.24E-05
Liver	1.23E-03	4.93E-05	1.13E-03	4.53E-05
Lungs	1.22E-03	1.46E-04	1.19E-03	1.43E-04
Pancreas	1.08E-03	9.95E-06	9.38E-04	8.66E-06
Prostate	9.28E-03	4.29E-05	2.78E-03	1.28E-05
Salivary Glands	7.03E-04	7.03E-06	7.01E-04	7.01E-06
Red Marrow	1.66E-03	1.99E-04	9.00E-04	1.08E-04
Osteogenic Cells	1.08E-03	1.08E-05	6.80E-04	6.80E-06
Spleen	1.08E-03	9.96E-06	9.86E-04	9.10E-06
Testes	2.65E-03	1.06E-04	1.13E-03	4.53E-05
Thymus	7.65E-04	7.06E-06	7.48E-04	6.90E-06
Thyroid	7.43E-04	2.97E-05	7.32E-04	2.93E-05
Urinary Bladder Wall	1.74E-01	6.96E-03	4.13E-02	1.65E-03
Total Body	2.20E-03	---	1.09E-03	---
Total Effective Dose (mSv/MBq)	---	8.17E-03	---	2.49E-03

current results in terms of biodistribution and dosimetry extrapolation.

The residence time in hours for mice organs is shown in Table 1. The bladder+urine, kidneys and carcass had high values. The highest value was observed for the remainder when the bladder+urine without bladder voiding was considered. The difference between bladder+urine residence time with and without bladder voiding is about four times.

Mass values for the male dosimetric model from OLINDA are shown in Table 2. The difference in mass between a human model and measured mice organs

is between two to four orders of magnitude. This table also shows the residence times for the human model. These figures were used in OLINDA to estimate the absorbed dose or the mean effective dose contributions per organ and for the whole body, and the highest values of residence time for the male dosimetric model were for the remainder, bladder+urine and kidneys.

Table 3 shows the results for absorbed and effective dose estimations with and without bladder voiding. The total absorbed dose varied between two to four times for organs close to the bladder content (small intestine, rectum, prostate and testes), indicating the importance of taking bladder voiding into account. In addition, it is important to note the difference in the total absorbed dose to the urinary bladder wall, which was about four times taking the same consideration into account. For organs far from the bladder content compartment, the values of the total absorbed dose were in the same order of magnitude. Regarding the mean effective dose, its difference was about three times.

As described by Ishiwata *et al*. and Tolvanen *et al*. in rats (19,36), it was verified that one of the organs with the highest total absorbed dose was the kidneys; for OLINDA, when bladder voiding was considered, it was 8.93 x 10^{-3} mGy/MBq, and without considering bladder voiding, it was 9.19 x 10^{-3} mGy/MBq.

The mean effective dose for OLINDA was 8.17 x 10^{-3} mSv/MBq and 2.49 x 10^{-3} mSv/MBq without and with the bladder voiding consideration, respectively. Tolvanen *et al*. (36) reported effective dose values varying from 3.2 x 10^{-3} to 1.41 x 10^{-2} mSv/MBq for ^{11}C-radiopharmaceuticals in humans, and the current results are comparable to these figures.

According to CUDIM protocols, the injected activity of this product will be between 4-6 MBq/kg, which translates to 292–438 MBq for a 73 kg patient. For OLINDA without bladder voiding, the effective dose range was between 2.38–3.58 mSv, and with bladder voiding, the effective dose ranged from 0.73–1.09 mSv.

In this work, the absorbed dose of major organs as well as the effective dose were extrapolated from animal measurements. One way to validate the extrapolated results in humans would be to perform dosimetry studies in humans.

4. Conclusions

The biological evaluation of [^{11}C]SAM in a healthy mice model was performed based on biodistribution and PET/CT studies. The highest tracer uptake was observed in the kidneys, bladder and urine. These results indicate a high elimination due to urinary excretion. A rapid blood clearance of the radiotracer was verified. The PC3 tumour-bearing mice biodistributions allowed for the evaluation of the tumour uptake of [^{11}C]SAM. Tumour accumulation was higher than that obtained for the contralateral muscle at all analysed times. The PET/CT studies showed a statistically higher *in vivo* tumour uptake of [^{11}C]SAM compared to [^{11}C]COL in the PC3 prostate cancer xenograft model. Absorbed dose estimations for major organs and the effective dose were determined. The results suggest that [^{11}C]SAM may be a potential prostate cancer imaging agent. To validate the extrapolated results in humans, dosimetry studies must be performed in humans.

Acknowledgements

The authors express their gratitude to the National Research and Innovation Agency (ANII) for a grant to Florencia Zoppolo as a research fellowship and to PEDECIBA-Química. Erick Mora Ramirez was partly funded by the University of Costa Rica (UCR), the French Institute for Central America (IFAC), the Cancer Research Centre of Toulouse (CRCT) and the French National Institute of Health and Medical Research (INSERM). This work was supported by CUDIM.

List of abbreviations

[^{11}C]COL, [^{11}C]choline
[^{18}F]FACBC, anti-1-amino-3-[^{18}F]-fluorocyclobutane-1-carboxylic acid
[^{18}F]FDHT, 16a-[^{18}F]-fluoro-5a-dihydrotestosterone
[^{18}F]FEC, [^{18}F]fluoroethylcholine
[^{18}F]PSMA, prostate-specific membrane antigen agents labelled with ^{18}F
[^{68}Ga]PSMA, prostate-specific membrane antigen agents labelled with ^{68}Ga
[^{177}Lu]PSMA-617, prostate-specific membrane antigen 617 labelled with ^{177}Lu
% A_{inj}, percentage of injected activity
% IA, percentage of injected activity in the whole organ

% IA/g, percentage of injected activity per gram of tissue
ANII, National Research and Innovation Agency
CEUA, commission of ethics for animal studies
CNEA, national commission of experimentation with animals
CRCT, Centre de Recherches en Cancérologie de Toulouse
CT, Computed tomography
CUDIM, Uruguayan Centre of Molecular Imaging
FBS, foetal bovine serum
FOV, field of view
GNMT, Glycine N-methyltransferase
ICRP, International commission on radiological protection
IFAC, French Institute for Central America
INSERM, Institut National de la Santé et de la Recherche Médicale
Iv, Intravenously
MIRD, Medical Internal Radiation Dose Committee
MLEM, maximum likelihood expectation maximisation
NURBS, Non-uniform rational B-spline
PCa, Prostate cancer
PET, Positron emission tomography
PSA, Prostate-specific antigen
PSMA, Prostate-specific membrane antigen
SAH, *S*-adenosyl homocysteine
SAM or AdoMet, *S*-adenosyl methionine
SD, standard deviation
SPECT, Single photon emission computed tomography
t_{inj}, injection time
t_{mes}, measuring time
t_{sac}, sacrifice time
T/NT, target to non-target
UCR, University of Costa Rica
UdelaR, Universidad de la República
VOIs, volumes of interest

References

1. Ferlay J, Soerjomataram I, Ervik M, Dikshit R, Eser S, Mathers C, et al. GLOBOCAN 2012 v1. 0, Cancer Incidence and Mortality Worldwide: IARC Cancer Base No. 11 2013; Lyon, France: International Agency for Research on Cancer.
2. Jadvar H. Prostate cancer: PET with 18F-FDG, 18F-or 11C-acetate, and 18F-or 11C-choline. J. Nucl. Med.; 2011;52(1):81–9. DOI: 10.2967/jnumed.110.077941
3. Schöder H, Larson SM. Positron emission tomography for prostate, bladder, and renal cancer. Semin. Nucl. Med. 2004;34(4):274–92.
4. Lee DJ, Mallin K, Graves AJ, Chang SS, Penson DF, Resnick MJ, et al. Recent Changes in Prostate Cancer Screening Practices and Epidemiology. J. Urol. 2017;198:1230–40. DOI: 10.1016/j.juro.2017.05.074
5. Williamson S. Prostate cancer: risk factors and diagosis. Clin. Pharm. 2015;7:127–30.
6. Williamson S. Prostate cancer: treatment options. Clin. Pharm. 2015;7:132–7.
7. Jadvar H. Prognostic utility of PET in prostate cancer. PET Clin. 2015;10(2):255-263. DOI: 10.1016/j.cpet.2014.12.007
8. Castellucci P, Ceci F, Graziani T, Juarez AR, Alvarez Nieto LF, Fanti S. PET/CT in prostate cancer. Médecine Nucléaire. 2015;39 (1):54–8. DOI: 10.1016/j.mednuc.2015.01.001
9. Mikla V, Mikla V. Medical Imaging Technology. Elsevier; 2014. 53-64 p.
10. Li Z, Conti PS. Radiopharmaceutical chemistry for positron emission tomography. Adv. Drug Deliv. Rev. 2010;62(11):1031–51. DOI: 10.1016/j.addr.2010.09.007
11. Ceci F, Fiorentino M, Castellucci P, Fanti S. Molecular Imaging and Precision Medicine in Prostate Cancer. PET Clin. Elsevier Inc; 2017;12(1):83–92. DOI: 10.1016/j.cpet.2016.08.004
12. Schuster D, Nanni C, Fanti S. PET Tracers Beyond FDG in Prostate Cancer. Semin Nucl Med. 2016;46(6):507–21. DOI: 10.1053/j.semnuclmed.2016.07.005
13. Rossi PJ, Schuster DM. Molecular imaging of advanced prostate cancer. Curr. Probl. Cancer. 2014;39(1):29–32. DOI: 10.1016/j.currproblcancer.2014.11.005
14. DeGrado TR, Baldwin SW, Wang S, Orr MD, Liao RP, Friedman HS, et al. Synthesis and evaluation of (18)F-labeled choline analogs as oncologic PET tracers. J. Nucl. Med. 2001;42(12):1805–14.
15. Mestre-Fusco A, Suárez-Piñera M. Use of choline tracers in the prostate carcinoma management. Médecine Nucléaire. 2013;37(3):71–7. DOI: 10.1016/j.mednuc.2012.11.004
16. Song YH, Shiota M, Kuroiwa K, Naito S, Oda Y. The important role of glycine N-methyltransferase in the

carcinogenesis and progression of prostate cancer. Mod. Pathol. 2011;24(9):1272–80. DOI: 10.1038/modpathol.2011.76
17. Sreekumar A, Poisson LM, Rajendiran TM, Khan AP, Cao Q, Yu J, et al. Metabolomic profiles delineate potential role for sarcosine in prostate cancer progression. Nature. 2009;457(7231):910–4. DOI: 10.1038/nature07762
18. Zoppolo F, Porcal W, Oliver P, Savio E, Engler H. Automated One-pot Radiosynthesis of [11C]S-adenosyl Methionine. Curr. Radiopharm. 2017;10(3):203–11. DOI: 10.2174/1874471010666170718171441
19. Ishiwata K, Ido T, Sato H, Iwata R, Kawashima K, Yanai K, et al. Simplified enzymatic synthesis and biodistribution of 11C-S-adenosyl-L- methionine. Eur J Nucl Med. 1986(11);11:449–52.
20. Ishiwata K, Ido T, Abe Y, Matsuzawa T, Iwata R. Tumor Uptake Studies of S-Adenosyl-L- [methyl-11C] Methionine L- [methyl-11C] Methionine. Nucl. Med. Biol. 1988;15(2):123–6.
21. Shao X, Hockley BG, Hoareau R, Schnau PL, Scott PJH. Fully automated preparation of [11C]choline and [18F]fluoromethylcholine using TracerLab synthesis modules and facilitated quality control using analytical HPLC. Appl. Radiat. Isot. 2011;69(2):403–9. DOI: 10.1016/j.apradiso.2010.09.022
22. Eckerman K, Endo A. MIRD: radionuclide data and decay schemes 2nd edn (Reston, VA: Society for Nuclear Medicine). 2008.
23. Kreimerman I, Mora-Ramirez E, Reyes AL, Bardies M, Savio E, Engler H. Dosimetry and toxicity studies of the novel sulfonamide derivative of Sulforhodamine 101([18F]SRF101) at a preclinical level. Curr. Radiopharm. 2018;11:1–9. DOI: 10.2174/1874471011666180830145304
24. Salabert A-S, Mora-Ramirez E, Beaurain M, Alonso M, Fontan C, Tahar HB, et al. Evaluation of [18 F] FNM biodistribution and dosimetry based on whole-body PET imaging of rats. Nucl. Med. Biol. Elsevier; 2018;59:1–8. DOI: 10.1016/j.nucmedbio.2017.12.003
25. Mathematica W. Wolfram Research. Inc., Champaign, Illinois. 2015.
26. McParland BJ. Nuclear Medicine Radiation Dosimetry: Advanced Theoretical Principles. Springer Science & Business Media; 2010. 519-531 p.
27. Stabin MG, Sparks RB, Crowe E. OLINDA/EXM: the second-generation personal computer software for internal dose assessment in nuclear medicine. J. Nucl. Med. 2005;46(6):1023–7.
28. Stabin M, Siegel JA. Radar Dose Estimate Report: a Compendium of Radiopharmaceutical Dose Estimates Based on Olinda/Exm Version 2.0. J. Nucl. Med. 2018;59(1):154–60. DOI: 10.2967/jnumed.117.196261
29. Stabin MG, Xu XG, Emmons MA, Segars WP, Shi C, Fernald MJ. RADAR Reference Adult, Pediatric, and Pregnant Female Phantom Series for Internal and External Dosimetry. J Nucl Med. 2012;53:1807–13. DOI: 10.2967/jnumed.112.106138
30. ICRP. ICRP 23: Report of the task group on reference man. Ann. ICRP. 1975;0–480.
31. ICRP. Basic anatomical and physiological data for use in radiological protection: reference values. A report of age- and gender-related differences in the anatomical and physiological characteristics of reference individuals. ICRP Publication 89. Ann. ICRP. 2002;32(3-4):5–265.
32. Stabin M, Emmons MA, Segars WP, Fernald M, Brill AB. ICRP - 89 based adult and pediatric phantom series. J. Nucl. Med. 2008;49(Supplement 1):14P.
33. ICRP. 1990 Recommendations of the International Commission on Radiological Protection. ICRP Publication 60. Ann. ICRP. ICRP21(1-3); 1991;21:1–201.
34. ICRP. ICRP-103. The 2007 recommendations of the International Commision on Radiological Protection. Ann. ICRP. 2007;2-4:1-334.
35. Hofman MS, Violet J, Hicks RJ, Ferdinandus J, Ping Thang S, Akhurst T, et al. [177Lu]-PSMA-617 radionuclide treatment in patients with metastatic castration-resistant prostate cancer (LuPSMA trial): a single-centre, single-arm, phase 2 study. Lancet Oncol. 2018;19:825–33. DOI: 10.1016/S1470-2045(18)30198-0
36. Tolvanen T, Yli-Kerttula T, Ujula T, Autio A, Lehikoinen P, Minn H, et al. Biodistribution and radiation dosimetry of [11C]choline: A comparison between rat and human data. Eur. J. Nucl. Med. Mol. Imaging. 2010;37(5):874–83. DOI: 10.1007/s00259-009-1346-z
37. Avila-Rodriguez MA, Rios C, Carrasco-Hernandez J, Manrique-Arias JC, Martinez-Hernandez R, García-Pérez FO, et al. Biodistribution and radiation dosimetry of [64Cu]copper dichloride: first-in-human study in healthy volunteers. EJNMMI Research; 2017;7(1):98. DOI: 10.1186/s13550-017-0346-4

Supplementary data
Materials and methods

The procedure described in section 2.8 used to determine the percentage of injected activity, residence time and absorbed dose calculations was followed to generate values used as input for OLINDA/EXM V1.0. As mentioned, both versions of OLINDA/EXM provide information regarding organs mass; however, OLINDA/EXM V1.0 does not provide information regarding human bladder contents mass.

The mice remainder residence time was calculated as the sum of residence times for blood, muscles, bones, stomach, carcass, intestine and bladder+urine. Therefore, for the human remainder residence time used for OLINDA/EXM V1.0, the same organs were considered.

Results and discussion

Table S1 shows the human and mouse organ mass used for the scaling process as well as the residence times used for OLINDA/EXM V1.0. The highest value for human residence times was for the remainder, which is obvious due to the factors considered.

Table S2 shows the absorbed and effective dose results, which are highly similar to those obtained without the bladder-voiding consideration. The mean effective dose was 2.27 x 10^{-3} mSv/MBq, which is comparable to the values reported by Tolvanen *et al*. (36). According to CUDIM protocols, the effective dose will vary from 0.66 to 0.99 mSv.

Table S1. Mass values used for mass scaling to determine male residence times.

Organ	OLINDA/EXM V1.0			
	M_{male} (g)	S-factor[A] (mGy/MBq-s)	M_{mouse} (g)	T_{male}(h)
Heart Wall	316	2.28E-4	0.1400	4.77E-04
Kidney	299	2.46E-4	0.4746	9.56E-03
Liver+ Gallbladder[B]	1920.5	4.65E-5	1.8355	4.46E-03
Lungs	1000	7.01E-5	0.2018	3.47E-03
Spleen	183	4.08E-4	0.1109	2.83E-04
Remainder	69981.5	---	34.1023	3.54E-01[C]
Whole Body	73700	1.62E-6	36.8650	-----

[A] S-factor refers to self–irradiation; [B] S-factor (self-irradiation) for liver only; [C] Remainder takes into account blood, muscles, bones, stomach, carcass, intestine and bladder+urine.

Table S2. Absorbed and effective dose estimation for adult male phantom from OLINDA/EXM V1.0.

Target Organ	Male – OLINDA/EXM V 1.0	
	Total (mGy/MBq)	Effective Dose ICRP-60 (mSv/MBq)
Adrenals	2.47E-03	6.18E-06
Brain	1.96E-03	4.91E-06
Breasts	1.83E-03	9.15E-05
Gallbladder Wall	2.43E-03	---
LLI Wall	2.48E-03	2.97E-04
Small Intestine	2.53E-03	6.33E-06
Stomach Wall	2.38E-03	2.86E-04
ULI Wall	2.48E-03	6.19E-06
Heart Wall	1.46E-03	---
Kidneys	9.43E-03	2.36E-04
Liver	1.53E-03	7.66E-05
Lungs	1.77E-03	2.12E-04
Muscle	2.12E-03	5.30E-06
Ovaries	2.54E-03	5.08E-04
Pancreas	2.53E-03	6.32E-06
Red Marrow	1.96E-03	2.35E-04
Osteogenic Cells	3.15E-03	3.15E-05
Skin	1.77E-03	1.77E-05
Spleen	1.54E-03	3.85E-06
Testes	2.12E-03	0.00E+00
Thymus	2.17E-03	5.42E-06
Thyroid	2.20E-03	1.10E-04
Urinary Bladder Wall	2.45E-03	1.22E-04
Uterus	2.56E-03	6.41E-06
Total Body	2.17E-03	---
Total Effective Dose (mSv/MBq)	---	2.27E-03